

Wetting Transition Energy Curves for a Droplet on a Square-Post Patterned Surface

Wei Gong¹, Yingqing Zu², Sheng Chen¹, Yuying Yan^{1*}

¹*Fluids & Thermal Engineering Research Group, Faculty of Engineering, University
of Nottingham, University Park, Nottingham, NG7 2RD, UK*

²*Department of Aeronautics and Astronautics, Fudan University, Shanghai, 200433, P.R.
China*

Abstract: Due to the property of water repellence, biomimetic superhydrophobic surfaces have been widely applied to green technologies, in turn inducing wider and deeper investigations on superhydrophobic surfaces. Theoretical, experimental and numerical studies on wetting transitions have been carried out by researchers, but the mechanism of wetting transitions between Cassie-Baxter state and Wenzel state, which is crucial to develop a stable superhydrophobic surface, is still not fully understood. In this paper, the free energy curves based on the transition processes are presented and discussed in detail. The existence of energy barriers with or without consideration of the gravity effect, and the irreversibility of wetting transition are discussed based on the presented energy curves. The energy curves show that different routes of the Cassie-to-Wenzel transition and the reverse transition are the main reason for the irreversibility. Numerical simulations are implemented via a phase field lattice Boltzmann method of large density ratio, and the simulation results show good consistency with the theoretical analysis.

Keywords: wetting transition, energy curves, lattice Boltzmann method

28 1 Introduction

29 Surface roughness, which can be found in the form of micro or hierarchical structures in nature,
30 has been widely investigated for its enhancement to hydrophobicity [1-4]. Through mimicking
31 natural superhydrophobic surfaces including plant leaves and animals such as lotus leaves, rice
32 leaves and water strider legs, manmade superhydrophobic surfaces via various of
33 methodologies have been presented and applied in industrial applications, for instance, coating,
34 self-cleaning surfaces, microfluidic devices with surface-tension-induced drop motion and so
35 forth [5, 6]. Among all the natural water-repellence examples, lotus leaves are the most
36 impressive for their superhydrophobic characteristic which is also known as “lotus effect”. Due
37 to the micrometre order length scales of the micro posts on the surfaces, the apparent contact
38 angle (APCA) of lotus leaves is approximately 160° while the hysteresis angle is just about 4°
39 [7].

40

41 As the wetting phenomena have been investigated over the past decades, significant progress
42 on theoretical models has also been achieved with considerable attention. The starting point of
43 wetting on an ideal rigid, flat and homogeneous surface is characterized by the well-known
44 Young’s Equation [8]:

$$45 \quad \cos\theta_Y = \frac{\sigma_{SG} - \sigma_{SL}}{\sigma_{LG}} \quad (1)$$

46 where σ is the surface tension which represents the energy per unit area of the interface
47 between solid/gas, solid/liquid or liquid/gas, and θ_Y is the Young’s contact angle. Young’s
48 Equation reveals the relationship between surface tensions and contact angle in the ideal
49 situation, however, it cannot be applied to most real surface conditions due to the existence of
50 surface roughness. For the surface roughness, a new correlation where the apparent contact
51 angle is related to surface roughness was presented by Wenzel [9]:

$$52 \quad \cos\theta_w = r \frac{\sigma_{SG} - \sigma_{SL}}{\sigma_{LG}} \quad (2)$$

53 which is also normally written as the following reformed equation:

$$54 \quad \cos\theta_w$$
$$55 \quad = r \cos\theta_Y \quad (3)$$

56 where r , the roughness parameter corresponding to the “roughness factor”, which is also
 57 referred to as roughness area ratio, denotes as the ratio of the actual surface area with respect
 58 to the projected structure surface, and θ_w is the Wenzel’s angle. The Wenzel equation is
 59 associated with the homogeneous wetting states, where the grooves caused by the surface
 60 roughness are penetrated with water. Apart from the homogeneous wetting state, there is
 61 another stable state, the heterogeneous wetting state, and the corresponding equation to the
 62 heterogeneous wetting regime was proposed by Cassie and Baxter [10]:

$$63 \quad \cos\theta_{CB} = f\cos\theta_Y + f - 1 \quad (4)$$

64 If the roughness ratio, r_f , the ratio of the actual wetted area over the projected area is
 65 considered, equation (4) can be modified to the following form [11]:

$$66 \quad \cos\theta_{CB} = r_f f \cos\theta_Y + f - 1 \quad (5)$$

67 where f is the area fraction on the horizontal projected plane of the liquid-solid contact area
 68 over the total area of solid-liquid and liquid-gas contact. Equation (5) would become the same
 69 form with Wenzel’s equation when $f = 1$ and $r_f = r$. By equating equation (3) and equation
 70 (5), the critical contact angle theoretically used to separate the two wetting states can be
 71 calculated as [12]:

$$72 \quad \cos\theta_C = \frac{1 - f}{r_f f - r} \quad (6)$$

73 It should be noted that when $\theta_C > 90^\circ$, both two wetting states exist. Then the homogeneous
 74 wetting state is preferable only if $\theta_Y < \theta_C$, otherwise the droplet stays at a heterogeneous
 75 wetting state, theoretically [13]. However, it has been observed that, even the Young’s angle is
 76 smaller than the critical angle, the Cassie-Baxter wetting state can exist, which means that
 77 Wenzel and Cassie Baxter states may stay on the same specific surface at the same time [14-
 78 18].

79

80 Bormashenko E. reviewed the main experimental and theoretical approaches to wetting
 81 transitions in 2010 and 2015 respectively [19, 20]. Experiments to study the wetting transitions
 82 were implemented by giving external factors such as pressure [21], initial velocity [22],
 83 evaporation of droplets [23], vibration [24], and electric field [25, 26]. And the role of gravity
 84 in wetting transitions was also discussed [11]. Neelesh A. Patankar [11] and Zu Y. et al [27]

85 theoretically analyzed the wetting transition from Cassie-Baxter state to Wenzel state from the
86 free energy point of view, and the energy barrier was discussed both in their work. Whyman G.
87 et al. [28] theoretically investigated the interfacial free energy and discussed the irreversibility
88 of Cassie-to-Wenzel transition. Ren W [29] computed the transition states, the energy barriers
89 and the minimum energy paths for Cassie-to-Wenzel transition using the string method. G.
90 Pashos et al. [30, 31] developed a numerical method to investigate the minimum energy paths
91 and the free energy changes were presented in their works. S. Prakash et al. [32] studied the
92 spontaneous recovery of superhydrophobicity on nanotextured surfaces using molecular
93 simulations. Bico J. et al. [33] and Aurbach D. et al. [34] studied the Cassie impregnating state
94 apart from the Cassie-Baxter state and Wenzel state, and Gibbs free energy curves of the three
95 wetting states were presented. In their work the impregnating state was observed via vibration
96 so that the liquid can impregnate the grooves outside of the droplet/solid interface. In this paper,
97 we focus on the transition between the more regular Cassie-Baxter and Wenzel wetting states.

98

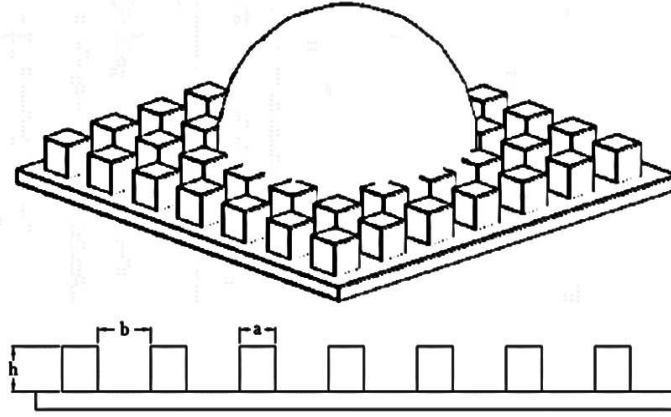
99 Wenzel's equation and Cassie and Baxter's equation can describe the stable wetting states on
100 real rough surfaces to a great extent when the droplet size is much larger than the typical
101 roughness scale. Nevertheless, there are still points of the theory of wetting states which are not
102 fully understood. For instance, when a droplet stays in a stable wetting state, and how the
103 transition between the two wetting states occurs [13]. It is crucial to understand the mechanism
104 of wetting transition process for the design and manufacturing of devices with highly stable
105 superhydrophobic surfaces. This paper focuses on the wetting transition process as well as the
106 different wetting states on the simplest model, the square-post patterned surface from the free
107 energy point of view.

108

109 **2 Theoretical analysis**

110 In the present study, the substrate patterned by square posts as the roughness surface is
111 considered as shown in Figure 1, where a , b and h are the post width, post spacing, and post
112 height respectively. It should be pointed out that the droplet size scale is much larger than the

113 size scale of micro posts in the theoretical analysis. Under this assumption, the theoretical
 114 analysis can be conducted based on a single unit of patterned substrate with periodical pattern
 115 and the Wenzel and Cassie-Baxter equations can be used for the calculation of the apparent
 116 contact angles. In the presented pattern, r_f equals to 1.



117
 118 Figure 1 Structure of the micro roughness surface
 119

120 2.1 The model of net free energy

121 All the parameters needed for the following theoretical analysis are presented in Figure 2 in
 122 three typical wetting state cases. Firstly, considering a droplet staying steady on a flat ideal
 123 surface as shown in Figure 2(a), the equilibrium free energy can be calculated as [13]:

$$124 \quad E_Y = S(\sigma_{SL} - \sigma_{SG}) + S'\sigma_{LG} \quad (7)$$

125 where S and S' represent the solid/liquid interface area and the liquid/gas interface area
 126 respectively. Similarly, the equilibrium free energy equations for Cassie-Baxter and Wenzel
 127 states are:

$$128 \quad 129 \quad E_{CB} = S_{CB}(\sigma'_{SL} - \sigma_{SG}) + S'_{CB}\sigma_{LG} \quad (8)$$

$$130 \quad E_W = S_W(\sigma'_{SL} - \sigma_{SG}) + S'_W\sigma_{LG} \quad (9)$$

131 where σ'_{SL} is the equivalent free energy per unit area of the solid/liquid interfaces for both of
 132 the two states, while S_{CB} and S_W both represent the projected horizontal areas. Considering
 133 the equivalent surface tension, Young's equation can be applied into the heterogeneous and
 134 homogeneous wetting states:

135 $\cos\theta_{CB}$
 136
$$= \frac{\sigma_{SG} - \sigma'_{SL}}{\sigma_{LG}} \tag{10}$$

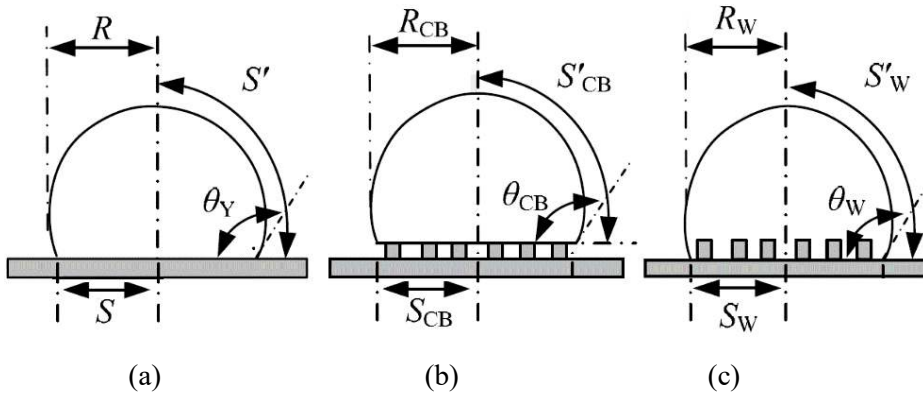
137 $\cos\theta_W$
 138
$$= \frac{\sigma_{SG} - \sigma'_{SL}}{\sigma_{LG}} \tag{11}$$

139 By combining the above equations, the free energy equations for Cassie-Baxter and Wenzel
 140 states can be expressed as:

141
$$E_{CB} = S_{CB}[f(\sigma_{SL} - \sigma_{SG}) + (1 - f)\sigma_{LG}] + S'_{CB}\sigma_{LG} \tag{12}$$

142
$$E_W = S_W r(\sigma_{SL} - \sigma_{SG}) + S'_W\sigma_{LG} \tag{13}$$

143
 144



145
 146 (a) (b) (c)
 147 Figure 2 Parameters of the droplet in (a) flat surface (b) Cassie-Baxter and (c) Wenzel
 148 state
 149

150 **2.2 Cassie-to-Wenzel wetting transition**

151 **2.2.1 Without gravity effects**

152 Usually, the transition process from Cassie-Baxter state to Wenzel state can be easily observed,
 153 however, the reverse process is hard to be achieved. Thus it is generally agreed that the wetting
 154 transition from Cassie-Baxter state to Wenzel state is irreversible [20]. Figure 3 shows the two
 155 main processes of wetting transition: (a) water starting to penetrate the posts intervals without
 156 touching the bottom surface; (b) water immersing the bottom surface. The position of the air
 157 pocket in Figure 3(b) can be neglected because the immersing-bottom process just lowers the

158 free energy and does not hinder the transition regarding the following analysis. \tilde{E}_{CB} and \tilde{E}_W
 159 are used to represent the intermediate free energy of the droplet. According to equation (7),
 160 there are:

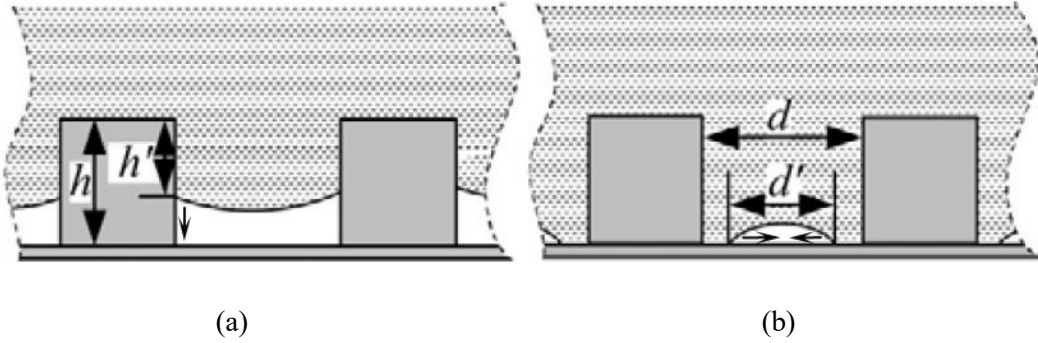
$$161 \quad \tilde{E}_{CB} = \tilde{S}_{CB} \left\{ \left[f + (r-1) \frac{h'}{h} \right] (\sigma_{SL} - \sigma_{SG}) + (1-f) \sigma_{LG} \right\} + \tilde{S}'_{CB} \sigma_{LG} \quad (14)$$

$$162 \quad \tilde{E}_W = \tilde{S}_W \left[r - (1-f) \frac{d'}{d} \right] (\sigma_{SL} - \sigma_{SG}) + \left[\tilde{S}'_W + \tilde{S}_W (1-f) \frac{d'}{d} \right] \sigma_{LG} \quad (15)$$

163 When h' and d' are on their extreme values h and d , the critical free energy states can be
 164 achieved:

$$165 \quad \hat{E}_{CB} = \hat{S}_{CB} \{ [f + (r-1)] (\sigma_{SL} - \sigma_{SG}) + (1-f) \sigma_{LG} \} + \hat{S}'_{CB} \sigma_{LG} \quad (16)$$

$$166 \quad \hat{E}_W = \hat{S}_W [r - (1-f)] (\sigma_{SL} - \sigma_{SG}) + [\hat{S}'_W + \hat{S}_W (1-f)] \sigma_{LG} \quad (17)$$



167
 168 (a) (b)
 169 Figure 3 Intermediate states for transition (a) water starting to penetrate the posts
 170 intervals without touching the bottom surface (b) water immersing the bottom surface

171
 172 It has been proved that the differences of the liquid/gas area and the droplet bottom projected
 173 area when transition happens are negligible owing to the much larger size scale compared to
 174 that of the surface roughness, which means $\hat{S}_{CB} \approx S_{CB}$, $\hat{S}_W \approx S_W$, $\hat{S}'_{CB} \approx S'_{CB}$ and $\hat{S}'_W \approx S'_W$
 175 [11, 35]. Hence there is $\hat{E}_{CB} = \hat{E}_W = E_{Cr}$ for the same droplet in different states. And the
 176 energy barriers for the two transitions process can be calculated as:

$$177 \quad E_{bar}^{CB-Cr} = \hat{E}_{CB} - E_{CB} = S_{CB} (r-1) (\sigma_{SL} - \sigma_{SG}) \quad (18)$$

$$178 \quad E_{bar}^{Cr-W} = E_W - \hat{E}_W = S_W (f-1) (\sigma_{LG} - \sigma_{SL} + \sigma_{SG}) \quad (19)$$

179
 180 For hydrophobic surfaces, i.e. $\theta_Y > 90^\circ$, according to the Young's equilibrium equation, there
 181 are $\sigma_{SL} - \sigma_{SG} > 0$ and $\sigma_{LG} - \sigma_{SL} + \sigma_{SG} > 0$, therefore

182

$$183 \quad E_{bar}^{CB-Cr} > 0 \quad (20)$$

$$185 \quad E_{bar}^{Cr-W} < 0 \quad (21)$$

187 Correspondingly, for hydrophilic water, i.e. $\theta_Y < 90^\circ$, there are $\sigma_{SL} - \sigma_{SA} < 0$ and $\sigma_{LA} - \sigma_{SL} + \sigma_{SA} > 0$, therefore

$$189 \quad E_{bar}^{CB-Cr} < 0 \quad (22)$$

$$191 \quad E_{bar}^{Cr-W} < 0 \quad (23)$$

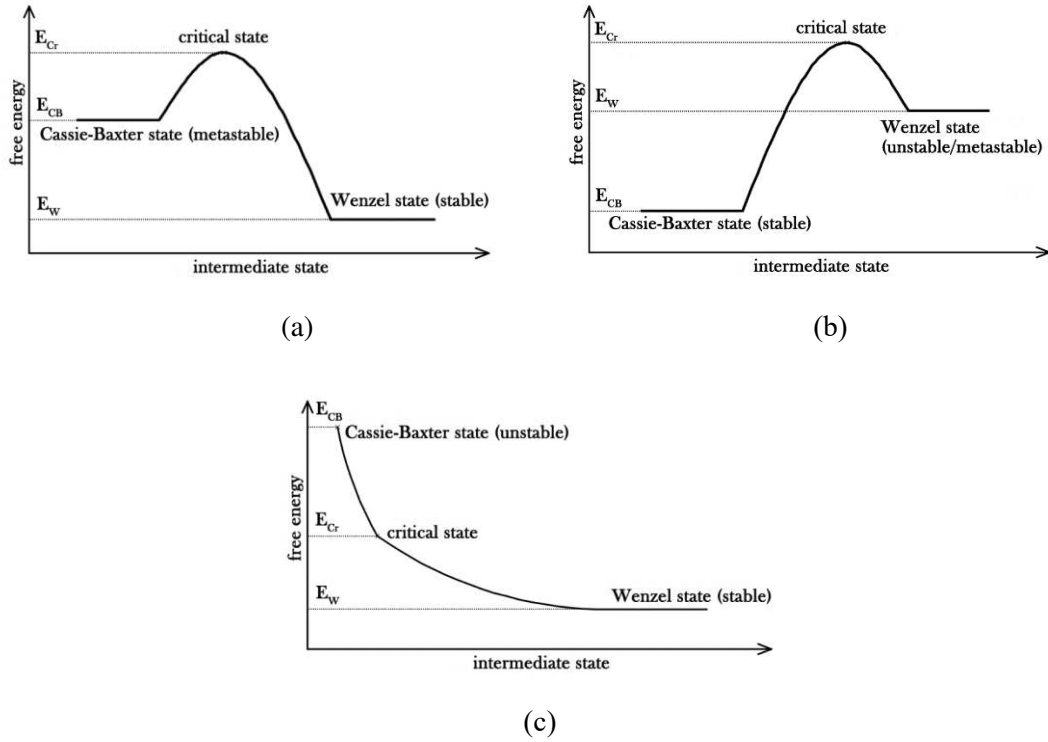
193 Whether the transition can occur depends on the sign of the differential of free energy at the beginning of the process. For transitions from Cassie-Baxter state to Wenzel state and the reverse, the free energy differentials can be given as:

$$196 \quad \left. \frac{\delta E^{CB-Cr}}{\delta h'} \right|_{h'=0} = \frac{S_{CB}(r-1)(\sigma_{SL} - \sigma_{SG})}{h} \quad (24)$$

197

198 Consequently, without considering the gravity effect or other external forces, the free energy curves can be drawn in Figure 4. Figure 4(a) and Figure 4(b) show the case of $\theta_Y > 90^\circ$, when two main roughness surface features exist: (a) $90^\circ < \theta_Y < \theta_C$, $E_{CB} > E_W$, according to the assumption that the equilibrium state occurs when the free energy is minimized [11], both of the two states exist, however, the Wenzel state is stable while Cassie-Baxter state is not; (b) $\theta_Y > \theta_C$, $E_W > E_{CB}$, the droplet would stay in the Cassie-Baxter state, but may not in the Wenzel state and the analysis relating to this is in the next section. This means the energy barrier always exists for the Cassie-to Wenzel transition for $\theta_Y > 90^\circ$. In addition, $\left. \frac{\delta E^{CB-W}}{\delta h'} \right|_{h'=0} > 0$ denotes that the transition processes cannot happen spontaneously without any external stimuli triggering event. Figure 4(c) indicates that Cassie-Baxter state cannot be achieved if $\theta_Y < 90^\circ$, when $E_{CB} > E_W$ and $\left. \frac{\delta E^{CB-W}}{\delta h'} \right|_{h'=0} < 0$ thus the droplet can only stays at the Wenzel state. It

209 should be noted that all the free energy curves presented in this paper are qualitatively
 210 constructed because there exist uncertainties for the wetting transitions, for example, the bottom
 211 droplet surface moving down along the posts is not definitely horizontal and when and which
 212 part of the droplet touches the bottom solid surface first is indeterminate.
 213



214
 215

216
 217

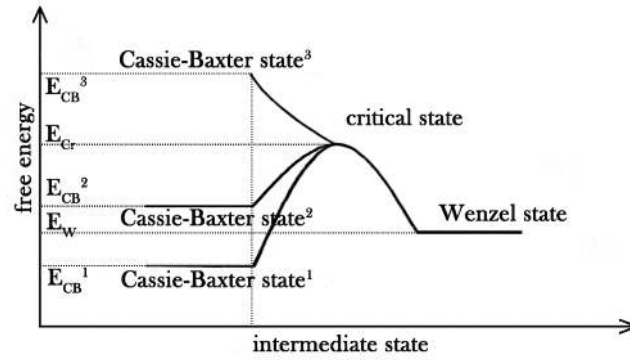
218 Figure 4 Free energy curves without gravity effect for (a) $90^\circ < \theta_Y < \theta_C$ (b) $\theta_Y > \theta_C$ and
 219 (c) $\theta_Y < 90^\circ$

220
 221

222 2.2.2 With gravity effects

223 The gravity does not affect the shape and the wetting state of a droplet significantly when the
 224 drop radius is much smaller than $(\sigma_{LA}/\rho g)^{1/2}$. However, its influence on transition may be
 225 nonnegligible [11]. When a droplet transits from the Cassie-Baxter state to the Wenzel state,
 226 the potential energy of gravity E_G declines as well. Since the potential energy change occurs
 227 along with the transition process between Cassie-Baxter state and the critical state when the
 228 droplet is about to immerse the air pockets completely but have not yet reached the bottom

229 surface, the energy curves can be modified by adding the potential energy change of which the
 230 sign is negative. When $\theta_Y < 90^\circ$, the energy curve is similar to Figure 4(c), where the energy
 231 change is monotonous. However, for $\theta_Y > 90^\circ$, one more case appears as shown in figure 5:



232

233 Figure 5 Energy curves with gravity effect for $\theta_Y > 90^\circ$

234

235 Figure 5 shows the extra curve of case 3 when considering the gravity effect with a monotonous
 236 energy change, which denotes that the transition can occur spontaneously. In this case, the
 237 source of potential energy change ΔE_G can overcome the energy barrier E_{bar}^{CB-Cr} , and the
 238 conclusion is the same with that from Patankar, N. A. [11] which is achieved via comparing the
 239 theoretical analysis with experimental data from Yoshimitsu et al [26].

240

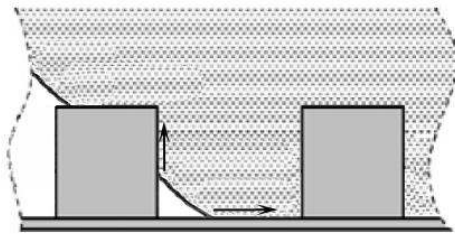
241 2.3 Discussion about the irreversibility of wetting transition

242 As mentioned above, it is generally thought that the transition from Cassie-Baxter state to
 243 Wenzel state is irreversible. From figure 5 it can be seen that the gravity potential energy can
 244 decrease the energy barrier E_{bar}^{CB-W} or even overcome it. Besides, other external stimuli such
 245 as initial velocity, pressure and vibration can also be used to overcome the energy barrier.
 246 Therefore, in most cases the Cassie-to-Wenzel transition is easier to be achieved, and more
 247 attention is paid on this transition due to its importance to superhydrophobic surfaces
 248 development.

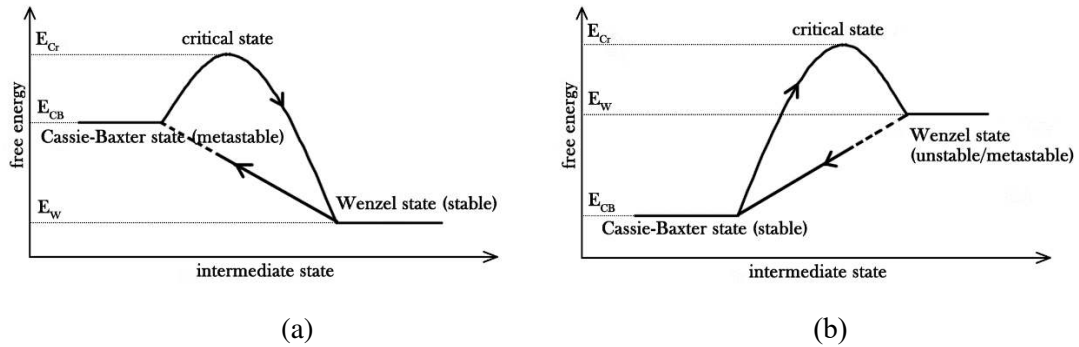
249

250 Without considering the gravity effect, the reverse Wenzel-to-Cassie transition would take a
 251 different route. It is reasonable to assume the transition happens on the bottom from the vicinity

252 of the gas-liquid-solid triple line, since air cannot be generated from the void, as shown in
 253 Figure 6. Therefore, the triple lines may move simultaneously in the horizontal and vertical
 254 directions. The energy decreased as solid-liquid contact area decreases may overcome the
 255 energy increased as liquid-gas contact area and solid-gas contact area increase, and if not, the
 256 reversible transition cannot occur spontaneously. Figure 6 presents the different routes of
 257 wetting transitions. It should be noticed that the reverse energy change may not be monotonous
 258 in Figure 7(a) in the case that the droplet is separated from the bottom but the vertical process
 259 has not finished yet, and in Figure 7(b) the critical Young's angle for the Wenzel-to-Cassie
 260 transition may not be the same with the critical angle in Equation (6).



261
 262 Figure 6 Intermediate states for Wenzel-to-Cassie transition
 263



264
 265 (a) (b)
 266 Figure 7 Free energy curves without gravity effect for (a) $90^\circ < \theta_Y < \theta_C$ (b) $\theta_Y > \theta_C$

267 Gravity potential can be considered as a part of the energy barrier needed to overcome.
 268 It is much more difficult to trigger the reverse transition than the Cassie-to-Wenzel
 269 transition due to the different transition routes, which can explain the irreversibility of
 270 wetting transition. Experiments to achieve the reverse transition were carried out by
 271 heating the substrate [36] or transmitting a short pulse of electrical current [26], and

272 both of the two experiments appeared to be conducted by the evaporation of the droplet
273 in the vicinity of their gas-liquid-solid triple line, changing liquid phase to vapor phase
274 to break the reverse energy barrier and complete the reverse transition. Thus a
275 metastable Cassie-Baxter wetting state can be achieved as shown in Figure 7(a).

276

277 The energy curves shown in Figure 7 can be very helpful to understand the wetting
278 transition mechanism and develop superhydrophobic surfaces. Some surfaces with
279 topographic features involving specialized geometries such as inverse trapezoidal [37],
280 T-shape [38] and serif-T [39] are the typical examples to impede Cassie-to-Wenzel
281 wetting transition by increasing the energy barrier during Cassie-to-critical process,
282 namely raising the critical state energy in Figure 7. However, few papers were found to
283 focus on the critical-to-Wenzel process, which could also be a crucial factor to affect
284 wetting transition because no matter how high the critical state energy is the Cassie-to-
285 Wenzel transition can be finished when the energy barrier is overcome by external
286 forces. Such work relating to the bottom surface as well as the critical-to-Wenzel
287 process will be investigated in the future.

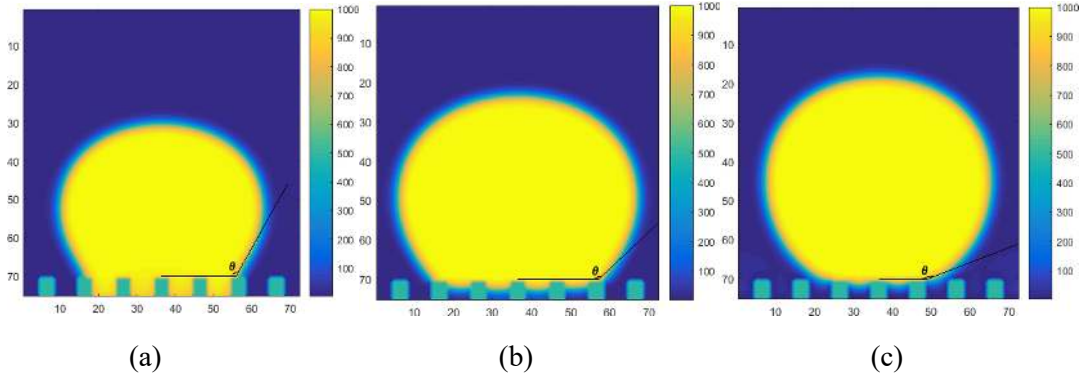
288

289 **3 Numerical simulation**

290 In this section, the simulation with a phase field lattice Boltzmann method with large density
291 ratio developed by Y. Q. Zu [40] is implemented to study the wetting states. As shown in Figure
292 8, a spherical water droplet with the initial radius $30\mu\text{m}$ is placed on the patterned surfaces in
293 different wetting states and different Young's contact angles. In the simulation, $a = d = h =$
294 $5\mu\text{m}$, and the critical Young's angle $\theta_c = 115.4^\circ$ calculated via equation (6). Young's angles
295 θ_Y of 105° and 130° are set for a Wenzel preferable and a Cassie-Baxter preferable states.
296 The water/gas properties are set naturally as: $\rho_L = 1000\text{kg}/\text{m}^3$, $\rho_G = 1.204\text{kg}/\text{m}^3$, $\mu_L =$
297 $1 \times 10^{-3}\text{kg}/(\text{m} \cdot \text{s})$, $\mu_G = 1.9 \times 10^{-5}\text{kg}/(\text{m} \cdot \text{s})$ for the density and dynamic viscosity,
298 respectively. Gravity is not considered in the simulation because it can be seen as an external
299 force to trigger the transition.

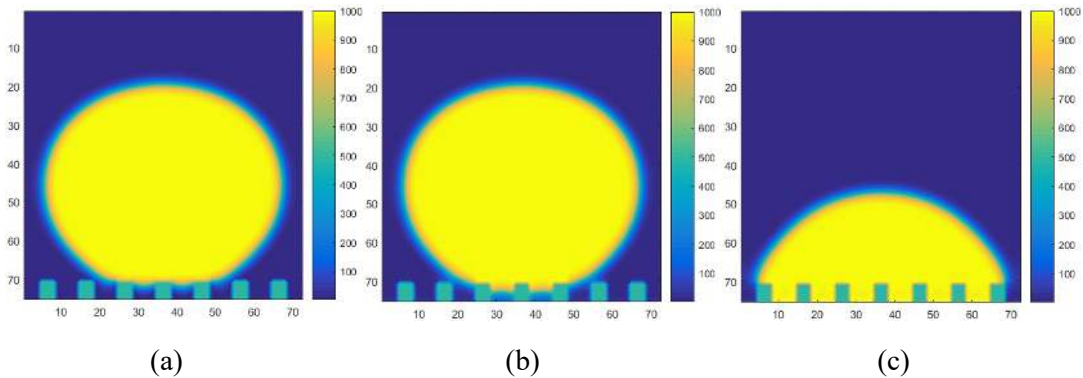
300

301 After evolving for $2,000,000\delta_t$ ($20ms$), where δ_t is the time step of LBM, all the droplets
302 go stable and the shapes of the droplets do not change anymore. Eventually, for $\theta_Y = 105^\circ$,
303 both Wenzel state and Cassie-Baxter state can be achieved with the apparent contact angles
304 119° and 137° , while for $\theta_Y = 130^\circ$, there is just the Cassie-Baxter state left, with $\theta_{CB} =$
305 158° . The apparent contact angles calculated by equation (3) and equation (5) are 121.2° ,
306 144.6° and 155.6° respectively, which are close to the present simulation data.



309 Figure 8 Wetting states for different Young's angles, $\theta_C = 115.4^\circ$, $t = 2,000,000\delta_t$ (a)
310 $\theta_Y = 105^\circ$, Wenzel state (b) $\theta_Y = 105^\circ$, Cassie-Baxter state (c) $\theta_Y = 130^\circ$, Cassie-Baxter
311 state

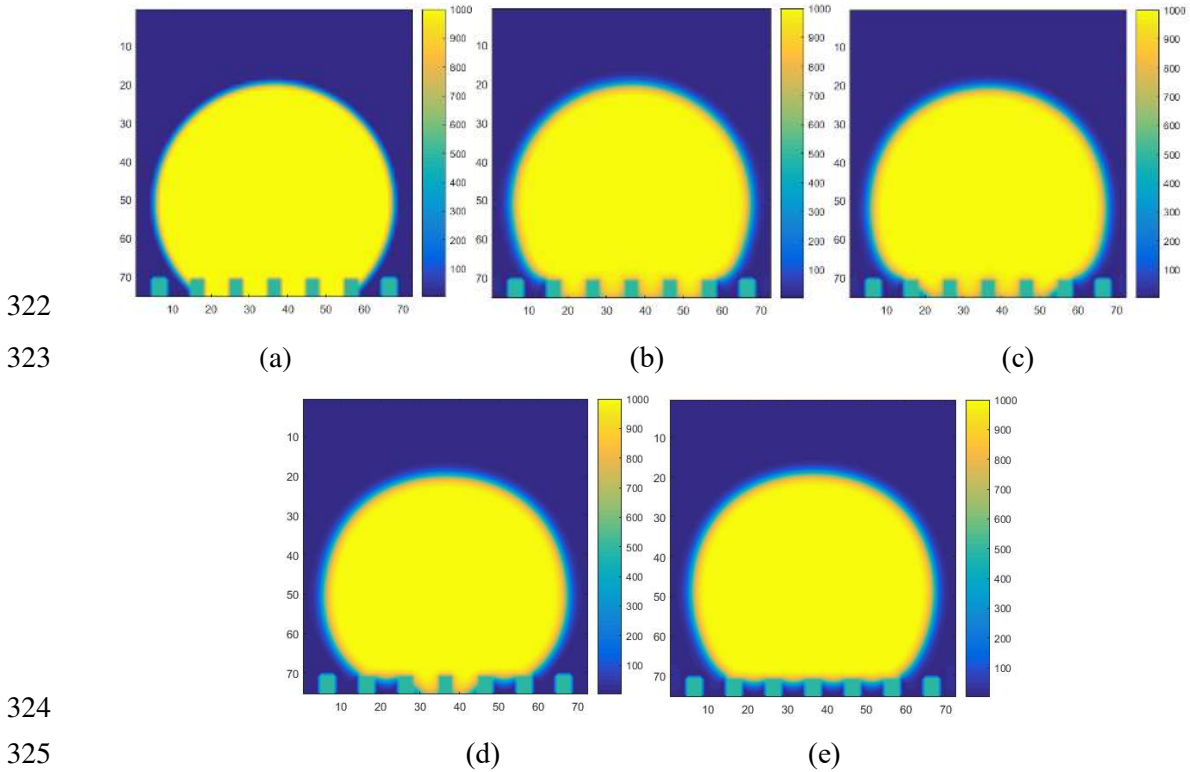
312 The dynamic wetting transition on an intrinsically hydrophilic surface with $\theta_Y = 75^\circ$ is
313 simulated, as shown in Figure 9. The stable Cassie-Baxter state cannot be observed as the
314 transition occurs spontaneously without any external forces.



317 Figure 9 Water spreading on the patterned surface for $\theta_Y = 75^\circ$ (a) $t = 0\delta_t$ (b) $t =$
318 $40,000\delta_t$ (c) $t = 700,000\delta_t$

319 Figure 10 shows the Wenzel-Cassie transition process of the droplet with Young's contact angle

320 of 130° being initially placed on the patterned surface in a Wenzel state. It can be clearly seen
 321 that the transition occurs on the patterned surface from the vicinity of the three phase line.



324
 325
 326 Figure 10 The Wenzel-Cassie transition for $\theta_Y = 130^\circ$ (a) $t = 0\delta_t$ (b) $t = 10,000\delta_t$
 327 (c) $t = 60,000\delta_t$ (d) $t = 130,000\delta_t$ (e) $t = 170,000\delta_t$

328 The simulations are in good agreement with the proposed energy curves. The droplet in Cassie-
 329 Baxter state in Figure 8(b) has a higher free energy compared to the droplet in Wenzel state, but
 330 it can keep steady, which means there is an energy barrier existing between the two wetting
 331 states. In addition, the simulation excludes the influence from the roughness of much smaller
 332 order of sizes which might be a factor to determine the two wetting state in experimental studies.
 333 When the intrinsic contact angle is 75° , smaller than 90° , there is no stable Cassie-Baxter state
 334 observed. The transition occurs spontaneously without any external forces, which means there
 335 is no energy barrier between the two wetting states. For a higher inherent contact angle $\theta_Y =$
 336 130° the Wenzel state in the simulation is unstable and the Wenzel-to-Cassie occurs
 337 spontaneously, confirming the reverse transition route in Figure 7(b). However, when testing
 338 some cases in which the Young's angles are between 130° and the critical angle, the reverse
 339 transition cannot be observed. This means the critical contact angle for Wenzel-to-Cassie

340 transition is not the same as the one determining the same energies of Cassie-Baxter state and
341 Wenzel state.

342

343

344 **4 Conclusions**

345 In this paper, the wetting transitions for a droplet on a square-post patterned surface are
346 theoretically analyzed. Numerical simulations with a phase field lattice Boltzmann method
347 were carried out, and the results show good agreement with the theoretical analysis. The main
348 finding of this work is that the energy curves during wetting transitions are proposed for Cassie-
349 to-Wenzel transition together with the reverse transition via the theoretical analysis of the free
350 energy changes during the transitions processes. The energy curves give a clear description of
351 the conditions in which the transitions occur and the energy barriers exist for both transition
352 processes. Gravity effect for wetting transition is considered, and the energy curves illustrate
353 that the gravity can be a driving force to trigger the transition. The irreversibility is discussed
354 based on the energy curves presented. The Wenzel-to-Cassie transition can occur spontaneously
355 only if the inherent contact angle is large enough. It can also be concluded from the curves that
356 different routes of the Cassie-to-Wenzel transition and the reverse transition are the main reason
357 for the irreversibility of wetting transitions. The work is based on the regular square-post
358 patterned surface, which is also the basis of most complicated rough surfaces. Therefore the
359 presented energy curves can be very helpful to understand the mechanism of complex wetting
360 phenomena.

361

362

363 **Acknowledgement**

364 The authors would like to acknowledge the financial support of this work by the doctoral degree
365 scholarship of China Scholarship Council and the University of Nottingham, UK.

366

367

368 **References**

369

- 370 1. Li L, Liu X, Dai X J, et al. (2013) Surface wetting processing on BNNT films by selective plasma
371 modes. *Chin Sci Bull* 58:3403-3408
- 372 2. Yao J, Wang J, Yu Y, et al. (2012) Biomimetic fabrication and characterization of an artificial rice
373 leaf surface with anisotropic wetting. *Chin Sci Bull* 57:2631-2634
- 374 3. Yao Z, Hao P, Zhang X, et al. (2012) Static and dynamic characterization of droplets on
375 hydrophobic surfaces. *Chin Sci Bull* 57:1095-1101
- 376 4. Yan Y (2009) Physical and numerical modelling of biomimetic approaches of natural
377 hydrophobic surfaces. *Chin Sci Bull* 54:541-548
- 378 5. Gao N, Yan Y, Chen X, et al. (2012) Nanoparticle-induced morphology and hydrophilicity of
379 structured surfaces. *Langmuir* 28:12256-65
- 380 6. Huang Y, Hu Y, Zhu C, et al. (2016) Long-Lived Multifunctional Superhydrophobic
381 Heterostructure Via Molecular Self-Supply. *Adv Mater Interfaces* 3:1500727
- 382 7. Koch K, Bhushan B, and Barthlott W (2009) Multifunctional surface structures of plants: an
383 inspiration for biomimetics. *Prog Mater Sci* 54:137-178
- 384 8. Young T (1805) An essay on the cohesion of fluids. *Philos Trans R Soc London* 95:65-87
- 385 9. Wenzel R N (1949) Surface Roughness and Contact Angle. *J Phys Chem* 53:1466-1467
- 386 10. Cassie A and Baxter S (1944) Wettability of porous surfaces. *Trans Faraday Society* 40:546-551
- 387 11. Patankar N A (2004) Transition between superhydrophobic states on rough surfaces. *Langmuir*
388 20:7097-7102
- 389 12. Gao N and Yan Y (2009) Modeling Superhydrophobic Contact Angles and Wetting Transition. *J*
390 *Bionic Eng* 6:335-340
- 391 13. Yan Y, Gao N, and Barthlott W (2011) Mimicking natural superhydrophobic surfaces and
392 grasping the wetting process: A review on recent progress in preparing superhydrophobic
393 surfaces. *Adv Colloid Interface Sci* 169:80-105
- 394 14. Marmur A and Bittoun E (2009) When Wenzel and Cassie are right: reconciling local and global
395 considerations. *Langmuir* 25:1277-1281
- 396 15. Marmur A (2008) From hydrophilic to superhydrophobic: theoretical conditions for making
397 high-contact-angle surfaces from low-contact-angle materials. *Langmuir* 24:7573-7579
- 398 16. Ran C, Ding G, Liu W, et al. (2008) Wetting on nanoporous alumina surface: transition between
399 Wenzel and Cassie states controlled by surface structure. *Langmuir* 24:9952-9955
- 400 17. Jung Y C and Bhushan B (2007) Wetting transition of water droplets on superhydrophobic
401 patterned surfaces. *Scripta Mater* 57:1057-1060
- 402 18. Koishi T, Yasuoka K, Fujikawa S, et al. (2009) Coexistence and transition between Cassie and
403 Wenzel state on pillared hydrophobic surface. *Proc Natl Acad Sci U S A* 106:8435-40
- 404 19. Bormashenko E (2010) Wetting transitions on biomimetic surfaces. *Philos Trans A Math Phys*
405 *Eng Sci* 368:4695-711
- 406 20. Bormashenko E (2015) Progress in understanding wetting transitions on rough surfaces. *Adv*
407 *Colloid Interface Sci* 222:92-103
- 408 21. Lafuma A and Quéré D (2003) Superhydrophobic states. *Nat Mater* 2:457-460
- 409 22. Jung Y C and Bhushan B (2009) Dynamic effects induced transition of droplets on biomimetic

410 superhydrophobic surfaces. *Langmuir* 25:9208-9218

411 23. McHale G, Aqil S, Shirtcliffe N, et al. (2005) Analysis of droplet evaporation on a
412 superhydrophobic surface. *Langmuir* 21:11053-11060

413 24. Bormashenko E, Pogreb R, Whyman G, et al. (2007) Resonance Cassie-Wenzel wetting
414 transition for horizontally vibrated drops deposited on a rough surface. *Langmuir* 23:12217-
415 12221

416 25. Bahadur V and Garimella S V (2008) Electrowetting-based control of droplet transition and
417 morphology on artificially microstructured surfaces. *Langmuir* 24:8338-8345

418 26. Krupenkin T N, Taylor J A, Wang E N, et al. (2007) Reversible wetting-dewetting transitions on
419 electrically tunable superhydrophobic nanostructured surfaces. *Langmuir* 23:9128-9133

420 27. Zu Y and Yan Y (2016) Single Droplet on Micro Square-Post Patterned Surfaces—Theoretical
421 Model and Numerical Simulation. *Sci Rep* 6:

422 28. Whyman G and Bormashenko E (2012) Wetting transitions on rough substrates: General
423 considerations. *J Adhes Sci Technol* 26:207-220

424 29. Ren W (2014) Wetting transition on patterned surfaces: transition states and energy barriers.
425 *Langmuir* 30:2879-85

426 30. Pashos G, Kokkoris G, and Boudouvis A G (2015) Minimum energy paths of wetting transitions
427 on grooved surfaces. *Langmuir* 31:3059-68

428 31. Pashos G, Kokkoris G, Papatthanasiou A G, et al. (2016) Wetting transitions on patterned
429 surfaces with diffuse interaction potentials embedded in a Young-Laplace formulation. *J Chem*
430 *Phys* 144:034105

431 32. Prakash S, Xi E, and Patel A J (2016) Spontaneous recovery of superhydrophobicity on
432 nanotextured surfaces. *Proc Natl Acad Sci* 201521753

433 33. Bico J, Thiele U, and Quéré D (2002) Wetting of textured surfaces. *Colloids Surf Physicochem*
434 *Eng Aspects* 206:41-46

435 34. Bormashenko E, Pogreb R, Stein T, et al. (2008) Characterization of rough surfaces with vibrated
436 drops. *Phys Chem Chem Phys* 10:4056-4061

437 35. Zu Y, Yan Y, Li J, et al. (2010) Wetting behaviours of a single droplet on biomimetic micro
438 structured surfaces. *J Bionic Eng* 7:191-198

439 36. Liu G, Fu L, Rode A V, et al. (2011) Water droplet motion control on superhydrophobic surfaces:
440 exploiting the Wenzel-to-Cassie transition. *Langmuir* 27:2595-2600

441 37. Im M, Im H, Lee J-H, et al. (2010) A robust superhydrophobic and superoleophobic surface with
442 inverse-trapezoidal microstructures on a large transparent flexible substrate. *Soft Matter*
443 6:1401-1404

444 38. Cai T-m, Jia Z-h, Yang H-n, et al. (2016) Investigation of Cassie-Wenzel Wetting transitions on
445 microstructured surfaces. *Colloid Polym Sci* 294:833-840

446 39. Liu T L and Kim C J (2014) Repellent surfaces. Turning a surface superrepellent even to
447 completely wetting liquids. *Science* 346:1096-100

448 40. Zu Y Q and Yan Y Y (2011) Lattice Boltzmann method for modelling droplets on chemically
449 heterogeneous and microstructured surfaces with large liquid-gas density ratio. *IMA J Appl*
450 *Math* 76:743-760

451